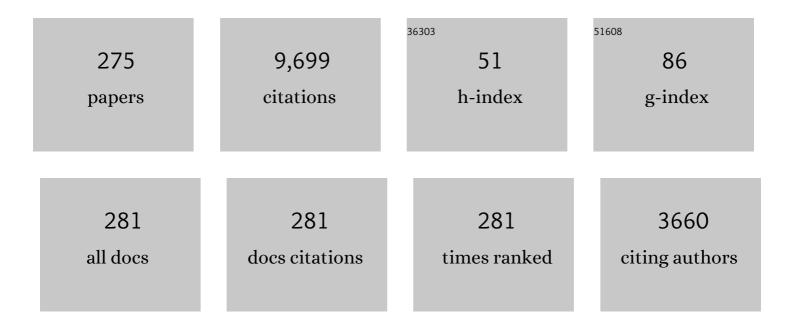
## **Gabriele Cremonese**

List of Publications by Year in descending order

Source: https://exaly.com/author-pdf/1926630/publications.pdf Version: 2024-02-01



#	Article	IF	CITATIONS
1	On the nucleus structure and activity of comet 67P/Churyumov-Gerasimenko. Science, 2015, 347, aaa1044.	12.6	366
2	Dust measurements in the coma of comet 67P/Churyumov-Gerasimenko inbound to the Sun. Science, 2015, 347, aaa3905.	12.6	310
3	OSIRIS – The Scientific Camera System Onboard Rosetta. Space Science Reviews, 2007, 128, 433-506.	8.1	286
4	The morphological diversity of comet 67P/Churyumov-Gerasimenko. Science, 2015, 347, aaa0440.	12.6	259
5	The global shape, density and rotation of Comet 67P/Churyumov-Gerasimenko from preperihelion Rosetta/OSIRIS observations. Icarus, 2016, 277, 257-278.	2.5	252
6	Shape model, reference system definition, and cartographic mapping standards for comet 67P/Churyumov-Gerasimenko – Stereo-photogrammetric analysis of Rosetta/OSIRIS image data. Astronomy and Astrophysics, 2015, 583, A33.	5.1	188
7	Spectrophotometric properties of the nucleus of comet 67P/Churyumov-Gerasimenko from the OSIRIS instrument onboard the ROSETTA spacecraft. Astronomy and Astrophysics, 2015, 583, A30.	5.1	188
8	Images of Asteroid 21 Lutetia: A Remnant Planetesimal from the Early Solar System. Science, 2011, 334, 487-490.	12.6	179
9	Insolation, erosion, and morphology of comet 67P/Churyumov-Gerasimenko. Astronomy and Astrophysics, 2015, 583, A34.	5.1	173
10	The primordial nucleus of comet 67P/Churyumov-Gerasimenko. Astronomy and Astrophysics, 2016, 592, A63.	5.1	159
11	Large heterogeneities in comet 67P as revealed by active pits from sinkhole collapse. Nature, 2015, 523, 63-66.	27.8	158
12	EVOLUTION OF THE DUST SIZE DISTRIBUTION OF COMET 67P/CHURYUMOV–GERASIMENKO FROM 2.2 au TO PERIHELION. Astrophysical Journal, 2016, 821, 19.	4.5	158
13	Regional surface morphology of comet 67P/Churyumov-Gerasimenko from Rosetta/OSIRIS images. Astronomy and Astrophysics, 2015, 583, A26.	5.1	153
14	A NEW CHRONOLOGY FOR THE MOON AND MERCURY. Astronomical Journal, 2009, 137, 4936-4948.	4.7	152
15	Redistribution of particles across the nucleus of comet 67P/Churyumov-Gerasimenko. Astronomy and Astrophysics, 2015, 583, A17.	5.1	149
16	Two independent and primitive envelopes of the bilobate nucleus of comet 67P. Nature, 2015, 526, 402-405.	27.8	141
17	Processes that Promote and Deplete the Exosphere ofÂMercury. Space Science Reviews, 2007, 132, 433-509.	8.1	121
18	E-Type Asteroid (2867) Steins as Imaged by OSIRIS on Board Rosetta. Science, 2010, 327, 190-193.	12.6	120

#	Article	IF	CITATIONS
19	Evidence for Young Volcanism on Mercury from the Third MESSENGER Flyby. Science, 2010, 329, 668-671.	12.6	118
20	Gravitational slopes, geomorphology, and material strengths of the nucleus of comet 67P/Churyumov-Gerasimenko from OSIRIS observations. Astronomy and Astrophysics, 2015, 583, A32.	5.1	113
21	The Colour and Stereo Surface Imaging System (CaSSIS) for the ExoMars Trace Gas Orbiter. Space Science Reviews, 2017, 212, 1897-1944.	8.1	111
22	Seasonal mass transfer on the nucleus of comet 67P/Chuyumov–Gerasimenko. Monthly Notices of the Royal Astronomical Society, 2017, 469, S357-S371.	4.4	111
23	Size-frequency distribution of boulders ≥7 m on comet 67P/Churyumov-Gerasimenko. Astronomy and Astrophysics, 2015, 583, A37.	5.1	108
24	The global meter-level shape model of comet 67P/Churyumov-Gerasimenko. Astronomy and Astrophysics, 2017, 607, L1.	5.1	107
25	Neutral Sodium from Comet Hale-Bopp: A Third Type of Tail. Astrophysical Journal, 1997, 490, L199-L202.	4.5	107
26	Are fractured cliffs the source of cometary dust jets? Insights from OSIRIS/Rosetta at 67P/Churyumov-Gerasimenko. Astronomy and Astrophysics, 2016, 587, A14.	5.1	102
27	The pristine interior of comet 67P revealed by the combined Aswan outburst and cliff collapse. Nature Astronomy, 2017, 1, .	10.1	100
28	OSIRIS observations of meter-sized exposures of H <sub>2</sub> O ice at the surface of 67P/Churyumov-Gerasimenko and interpretation using laboratory experiments. Astronomy and Astrophysics, 2015, 583, A25.	5.1	97
29	Rosetta's comet 67P/Churyumov-Gerasimenko sheds its dusty mantle to reveal its icy nature. Science, 2016, 354, 1566-1570.	12.6	97
30	Regional surface morphology of comet 67P/Churyumov-Gerasimenko from Rosetta/OSIRIS images: The southern hemisphere. Astronomy and Astrophysics, 2016, 593, A110.	5.1	86
31	The rotation state of 67P/Churyumov-Gerasimenko from approach observations with the OSIRIS cameras on Rosetta. Astronomy and Astrophysics, 2014, 569, L2.	5.1	81
32	Surface-Exosphere-Magnetosphere System Of Mercury. Space Science Reviews, 2005, 117, 397-443.	8.1	76
33	Flux of meteoroid impacts on Mercury. Astronomy and Astrophysics, 2005, 431, 1123-1127.	5.1	71
34	Fractures on comet 67P/Churyumovâ€Gerasimenko observed by Rosetta/OSIRIS. Geophysical Research Letters, 2015, 42, 5170-5178.	4.0	71
35	SIMBIO-SYS: The spectrometer and imagers integrated observatory system for the BepiColombo planetary orbiter. Planetary and Space Science, 2010, 58, 125-143.	1.7	70
36	Scientific assessment of the quality of OSIRIS images. Astronomy and Astrophysics, 2015, 583, A46.	5.1	67

#	Article	IF	CITATIONS
37	Detection of exposed H <sub>2</sub> O ice on the nucleus of comet 67P/Churyumov-Gerasimenko. Astronomy and Astrophysics, 2016, 595, A102.	5.1	67
38	Surface changes on comet 67P/Churyumov-Gerasimenko suggest a more active past. Science, 2017, 355, 1392-1395.	12.6	63
39	67P/Churyumov-Gerasimenko: Activity between March and June 2014 as observed from Rosetta/OSIRIS. Astronomy and Astrophysics, 2015, 573, A62.	5.1	60
40	Temporal morphological changes in the Imhotep region of comet 67P/Churyumov-Gerasimenko. Astronomy and Astrophysics, 2015, 583, A36.	5.1	60
41	The 2016 Feb 19 outburst of comet 67P/CG: an ESA Rosetta multi-instrument study. Monthly Notices of the Royal Astronomical Society, 2016, 462, S220-S234.	4.4	60
42	Origin of the local structures at the Philae landing site and possible implications on the formation and evolution of 67P/Churyumov–Gerasimenko. Monthly Notices of the Royal Astronomical Society, 2016, 462, S23-S32.	4.4	60
43	Geomorphology of the Imhotep region on comet 67P/Churyumov-Gerasimenko from OSIRIS observations. Astronomy and Astrophysics, 2015, 583, A35.	5.1	59
44	The geomorphology of (21) Lutetia: Results from the OSIRIS imaging system onboard ESA's Rosetta spacecraft. Planetary and Space Science, 2012, 66, 96-124.	1.7	58
45	The dust environment of comet 67P/Churyumov-Gerasimenko. Astronomy and Astrophysics, 2004, 422, 357-368.	5.1	58
46	Sunset jets observed on comet 67P/Churyumov-Gerasimenko sustained by subsurface thermal lag. Astronomy and Astrophysics, 2016, 586, A7.	5.1	55
47	Statistical analysis of micrometeoroids flux on Mercury. Astronomy and Astrophysics, 2009, 503, 259-264.	5.1	54
48	Comet 67P/Churyumov-Gerasimenko: Constraints on its origin from OSIRIS observations. Astronomy and Astrophysics, 2015, 583, A44.	5.1	53
49	Aswan site on comet 67P/Churyumov-Gerasimenko: Morphology, boulder evolution, and spectrophotometry. Astronomy and Astrophysics, 2016, 592, A69.	5.1	53
50	Mercury's Surface Composition and Character as Measured by Ground-Based Observations. Space Science Reviews, 2007, 132, 399-431.	8.1	52
51	Acceleration of individual, decimetre-sized aggregates in the lower coma of comet 67P/Churyumov–Gerasimenko. Monthly Notices of the Royal Astronomical Society, 2016, 462, S78-S88.	4.4	52
52	Spin Temperatures of Ammonia and Water Molecules in Comets. Astrophysical Journal, 2004, 601, 1152-1158.	4.5	51
53	The effects of the target material properties and layering on the crater chronology: The case of Raditladi and Rachmaninoff basins on Mercury. Planetary and Space Science, 2011, 59, 1968-1980.	1.7	51
54	Release of neutral sodium atoms from the surface of Mercury induced by meteoroid impacts. Icarus, 2005, 177, 122-128.	2.5	49

#	Article	IF	CITATIONS
55	Discovery of the Atomic Iron Tail of Comet M c Naught Using the Heliospheric Imager on STEREO. Astrophysical Journal, 2007, 661, L93-L96.	4.5	48
56	The Leonid Meteor Shower and the Lunar Sodium Atmosphere. Icarus, 1998, 136, 298-303.	2.5	47
57	SIMBIO-SYS: Scientific Cameras and Spectrometer for the BepiColombo Mission. Space Science Reviews, 2020, 216, 1.	8.1	47
58	Possible detection of meteor stream effects on the lunar sodium atmosphere. Planetary and Space Science, 1998, 46, 1003-1006.	1.7	46
59	The cratering history of asteroid (2867) Steins. Planetary and Space Science, 2010, 58, 1116-1123.	1.7	46
60	Rationale for BepiColombo Studies of Mercury's Surface and Composition. Space Science Reviews, 2020, 216, 1.	8.1	46
61	Evidence of sub-surface energy storage in comet 67P from the outburst of 2016 July 03. Monthly Notices of the Royal Astronomical Society, 2017, 469, s606-s625.	4.4	45
62	The scattering phase function of comet 67P/Churyumov–Gerasimenko coma as seen from the Rosetta/OSIRIS instrument. Monthly Notices of the Royal Astronomical Society, 2017, 469, S404-S415.	4.4	44
63	The BepiColombo mission: An outstanding tool for investigating the Hermean environment. Planetary and Space Science, 2010, 58, 40-60.	1.7	43
64	Seasonal erosion and restoration of the dust cover on comet 67P/Churyumov-Gerasimenko as observed by OSIRIS onboard Rosetta. Astronomy and Astrophysics, 2017, 604, A114.	5.1	43
65	Dust mass distribution around comet 67P/Churyumov–Gerasimenko determined via parallax measurements using Rosetta's OSIRIS cameras. Monthly Notices of the Royal Astronomical Society, 2017, 469, S276-S284.	4.4	43
66	Variegation of comet 67P/Churyumov-Gerasimenko in regions showing activity. Astronomy and Astrophysics, 2016, 586, A80.	5.1	43
67	PHEBUS: A double ultraviolet spectrometer to observe Mercury's exosphere. Planetary and Space Science, 2010, 58, 201-223.	1.7	42
68	Geological map and stratigraphy of asteroid 21 Lutetia. Planetary and Space Science, 2012, 66, 125-136.	1.7	42
69	Geomorphology and spectrophotometry of Philae's landing site on comet 67P/Churyumov-Gerasimenko. Astronomy and Astrophysics, 2015, 583, A41.	5.1	41
70	The pebbles/boulders size distributions on Sais: Rosetta's final landing site on comet 67P/Churyumov–Gerasimenko. Monthly Notices of the Royal Astronomical Society, 2017, 469, S636-S645.	4.4	40
71	Tensile strength of 67P/Churyumov–Gerasimenko nucleus material from overhangs. Astronomy and Astrophysics, 2018, 611, A33.	5.1	40
72	Mercury's radius change estimates revisited using MESSENGER data. Icarus, 2012, 221, 456-460.	2.5	39

#	Article	IF	CITATIONS
73	Large-scale dust jets in the coma of 67P/Churyumov-Gerasimenko as seen by the OSIRIS instrument onboard Rosetta. Astronomy and Astrophysics, 2015, 583, A9.	5.1	39
74	The dust environment of comet 67P/Churyumov-Gerasimenko from Rosetta OSIRIS and VLT observations in the 4.5 to 2.9 AU heliocentric distance range inbound. Astronomy and Astrophysics, 2016, 587, A155.	5.1	39
75	Thermal modelling of water activity on comet 67P/Churyumov-Gerasimenko with global dust mantle and plural dust-to-ice ratio. Monthly Notices of the Royal Astronomical Society, 2017, 469, S295-S311.	4.4	39
76	The distant activity of short-period comets – I. Monthly Notices of the Royal Astronomical Society, 2007, 381, 713-722.	4.4	37
77	The Preperihelion Dust Environment of C/1995 O1 Hale-Bopp from 13 to 4 AU. Astronomical Journal, 1998, 116, 1470-1477.	4.7	36
78	CHANGES IN THE PHYSICAL ENVIRONMENT OF THE INNER COMA OF 67P/CHURYUMOV–GERASIMENKO WITH DECREASING HELIOCENTRIC DISTANCE. Astronomical Journal, 2016, 152, 130.	4.7	36
79	Morphological and Spectral Diversity of the Clay-Bearing Unit at the ExoMars Landing Site Oxia Planum. Astrobiology, 2021, 21, 464-480.	3.0	35
80	Shortâ€ŧerm variations of Mercury's Na exosphere observed with very high spectral resolution. Geophysical Research Letters, 2009, 36, .	4.0	34
81	Gas outflow and dust transport of comet 67P/Churyumov–Gerasimenko. Monthly Notices of the Royal Astronomical Society, 2016, 462, S533-S546.	4.4	34
82	Observations and analysis of a curved jet in the coma of comet 67P/Churyumov-Gerasimenko. Astronomy and Astrophysics, 2016, 588, L3.	5.1	34
83	Experimental phase function and degree of linear polarization of cometary dust analogues. Monthly Notices of the Royal Astronomical Society, 2019, 484, 2198-2211.	4.4	34
84	The distant activity of Short Period Comets <sup>â~</sup> - II Monthly Notices of the Royal Astronomical Society, 2008, 390, 265-280.	4.4	33
85	High latitude peaks in Mercury's sodium exosphere: Spectral signature using THEMIS solar telescope. Geophysical Research Letters, 2008, 35, .	4.0	33
86	Morphology and dynamics of the jets of comet 67P/Churyumov-Gerasimenko: Early-phase development. Astronomy and Astrophysics, 2015, 583, A11.	5.1	33
87	Constraints on cometary surface evolution derived from a statistical analysis of 67P's topography. Monthly Notices of the Royal Astronomical Society, 2017, 469, S329-S338.	4.4	33
88	Meter-scale thermal contraction crack polygons on the nucleus of comet 67P/Churyumov-Gerasimenko. Icarus, 2018, 301, 173-188.	2.5	33
89	Optical design of the single-detector planetary stereo camera for the BepiColombo European Space Agency mission to Mercury. Applied Optics, 2010, 49, 2910.	2.1	32
90	Regional unit definition for the nucleus of comet 67P/Churyumov-Gerasimenko on the SHAP7 model. Planetary and Space Science, 2018, 164, 19-36.	1.7	32

#	Article	IF	CITATIONS
91	Mercury's exosphere origins and relations to its magnetosphere and surface. Planetary and Space Science, 2007, 55, 1069-1092.	1.7	30
92	The highly active Anhur–Bes regions in the 67P/Churyumov–Gerasimenko comet: results from OSIRIS/ROSETTA observations. Monthly Notices of the Royal Astronomical Society, 2017, 469, S93-S107.	4.4	30
93	A mini outburst from the nightside of comet 67P/Churyumov-Gerasimenko observed by the OSIRIS camera on Rosetta. Astronomy and Astrophysics, 2016, 596, A89.	5.1	29
94	The dust coma of the active Centaur P/2004 A1 (LONEOS): a CO-driven environment?. Astronomy and Astrophysics, 2006, 460, 935-944.	5.1	28
95	yThe Mercury sodium atmospheric spectral imager for the MMO spacecraft of Bepi-Colombo. Planetary and Space Science, 2010, 58, 224-237.	1.7	28
96	Neutral sodium atoms release from the surfaces of the Moon and Mercury induced by meteoroid impacts. Planetary and Space Science, 2007, 55, 1494-1501.	1.7	27
97	Observations of Comet 9P/Tempel 1 around the Deep Impact event by the OSIRIS cameras onboard Rosetta. Icarus, 2007, 187, 87-103.	2.5	27
98	NEW CALIBRATION OF THE MICROMETEOROID FLUX ON EARTH. Astrophysical Journal Letters, 2012, 749, L40.	8.3	27
99	Geologic mapping of the Comet 67P/Churyumov–Gerasimenko's Northern hemisphere. Monthly Notices of the Royal Astronomical Society, 2016, 462, S352-S367.	4.4	27
100	The southern hemisphere of 67P/Churyumov-Gerasimenko: Analysis of the preperihelion size-frequency distribution of boulders ≥7 m. Astronomy and Astrophysics, 2016, 592, L2.	5.1	27
101	High resolution observations of the sodium emission from the Moon. Advances in Space Research, 1997, 19, 1561-1569.	2.6	26
102	Rotating dust particles in the coma of comet 67P/Churyumov-Gerasimenko. Astronomy and Astrophysics, 2015, 583, A14.	5.1	26
103	Phobos grooves and impact craters: A stereographic analysis. Icarus, 2015, 256, 90-100.	2.5	26
104	Characterization of the Abydos region through OSIRIS high-resolution images in support of CIVA measurements. Astronomy and Astrophysics, 2016, 585, L1.	5.1	26
105	Decimetre-scaled spectrophotometric properties of the nucleus of comet 67P/Churyumov–Gerasimenko from OSIRIS observations. Monthly Notices of the Royal Astronomical Society, 2016, 462, S287-S303.	4.4	26
106	Timescales of the Climate Record in the South Polar Ice Cap of Mars. Geophysical Research Letters, 2019, 46, 7268-7277.	4.0	26
107	SERENA: Particle Instrument Suite for Determining the Sun-Mercury Interaction from BepiColombo. Space Science Reviews, 2021, 217, 11.	8.1	26
108	The distant activity of the Long Period Comets C/2003 O1 (LINEAR) and C/2004 K1 (Catalina). Astronomy and Astrophysics, 2009, 502, 355-365.	5.1	25

#	Article	IF	CITATIONS
109	Inflated flows on Daedalia Planum (Mars)? Clues from a comparative analysis with the Payen volcanic complex (Argentina). Planetary and Space Science, 2009, 57, 556-570.	1.7	25
110	Asteroidal and cometary dust flux in the inner solar system. Astronomy and Astrophysics, 2017, 605, A94.	5.1	24
111	Long-term survival of surface water ice on comet 67P. Monthly Notices of the Royal Astronomical Society, 2017, 469, S582-S597.	4.4	24
112	Image Simulation and Assessment of the Colour and Spatial Capabilities of the Colour and Stereo Surface Imaging System (CaSSIS) on the ExoMars Trace Gas Orbiter. Space Science Reviews, 2018, 214, 1.	8.1	24
113	Osiris—The optical, spectroscopic and infrared remote imaging system for the Rosetta Orbiter. Advances in Space Research, 1998, 21, 1505-1515.	2.6	23
114	Mercury's geochronology revised by applying Model Production Function to Mariner 10 data: Geological implications. Geophysical Research Letters, 2009, 36, .	4.0	23
115	Method for studying the effects of thermal deformations on optical systems for space application. Applied Optics, 2011, 50, 2836.	2.1	23
116	Orbital elements of the material surrounding comet 67P/Churyumov-Gerasimenko. Astronomy and Astrophysics, 2015, 583, A16.	5.1	23
117	Sublimation of icy aggregates in the coma of comet 67P/Churyumov–Gerasimenko detected with the OSIRIS cameras on board <i>Rosetta</i> . Monthly Notices of the Royal Astronomical Society, 2016, 462, S57-S66.	4.4	23
118	Geomorphological mapping of comet 67P/Churyumov–Gerasimenko's Southern hemisphere. Monthly Notices of the Royal Astronomical Society, 2016, 462, S573-S592.	4.4	23
119	Investigating the physical properties of outbursts on comet 67P/Churyumov–Gerasimenko. Monthly Notices of the Royal Astronomical Society, 2017, 469, S731-S740.	4.4	23
120	Mercury Hollows as Remnants of Original Bedrock Materials and Devolatilization Processes: A Spectral Clustering and Geomorphological Analysis. Journal of Geophysical Research E: Planets, 2018, 123, 2365-2379.	3.6	23
121	Physical properties and dynamical relation of the circular depressions on comet 67P/Churyumov-Gerasimenko. Astronomy and Astrophysics, 2016, 591, A132.	5.1	22
122	The opposition effect of 67P/Churyumov–Gerasimenko on post-perihelion Rosetta images. Monthly Notices of the Royal Astronomical Society, 2017, 469, S550-S567.	4.4	22
123	A three-dimensional modelling of the layered structure of comet 67P/Churyumov-Gerasimenko. Monthly Notices of the Royal Astronomical Society, 2017, 469, S741-S754.	4.4	22
124	Bilobate comet morphology and internal structure controlled by shear deformation. Nature Geoscience, 2019, 12, 157-162.	12.9	22
125	The 1999 Quadrantids and the lunar Na atmosphere. Monthly Notices of the Royal Astronomical Society, 2001, 327, 244-248.	4.4	21
126	Using Process Simulators for Steady-State and Dynamic Plant Analysis. Chemical Engineering Research and Design, 2004, 82, 499-512.	5.6	21

#	Article	IF	CITATIONS
127	On deviations from free-radial outflow in the inner coma of comet 67P/Churyumov–Gerasimenko. Icarus, 2018, 311, 1-22.	2.5	21
128	Spectrophotometry of the Khonsu region on the comet 67P/Churyumov–Gerasimenko using OSIRIS instrument images. Monthly Notices of the Royal Astronomical Society, 2016, 462, S274-S286.	4.4	20
129	The phase function and density of the dust observed at comet 67P/Churyumov–Gerasimenko. Monthly Notices of the Royal Astronomical Society, 2018, 476, 2835-2839.	4.4	20
130	Models of Rosetta/OSIRIS 67P Dust Coma Phase Function. Astronomical Journal, 2018, 156, 237.	4.7	20
131	O(\$^{mathsf 1}\$S) and O(\$^{mathsf 1}\$D) emission lines in the spectrum of 153P/2002 C1 (Ikeya-Zhang). Astronomy and Astrophysics, 2005, 442, 1121-1126.	5.1	20
132	Multicolor Photometry of the Uranus Irregular Satellites Sycorax and Caliban. Astronomical Journal, 2001, 121, 2800-2803.	4.7	19
133	Estimate of the neutral atoms' contribution to the Mercury exosphere caused by a new flux of micrometeoroids. Astronomy and Astrophysics, 2010, 517, A89.	5.1	19
134	Micrometeoroids flux on the Moon. Astronomy and Astrophysics, 2013, 551, A27.	5.1	19
135	Coma morphology of comet 67P controlled by insolation over irregular nucleus. Nature Astronomy, 2018, 2, 562-567.	10.1	19
136	Comparative study of water ice exposures on cometary nuclei using multispectral imaging data. Monthly Notices of the Royal Astronomical Society, 2016, 462, S394-S414.	4.4	18
137	Linking surface morphology, composition, and activity on the nucleus of 67P/Churyumov-Gerasimenko. Astronomy and Astrophysics, 2019, 630, A7.	5.1	18
138	Dust Environment Model of the Interstellar Comet 21/Borisov. Astrophysical Journal Letters, 2020, 893, L12.	8.3	18
139	Neutral sodium tails in comets. Advances in Space Research, 2002, 29, 1187-1197.	2.6	17
140	Catalog of the emission lines in the visible spectrum of comet 153P/Ikeya-Zhang. Astronomy and Astrophysics, 2007, 461, 789-792.	5.1	17
141	Post-perihelion photometry of dust grains in the coma of 67P Churyumov–Gerasimenko. Monthly Notices of the Royal Astronomical Society, 2017, 469, S195-S203.	4.4	17
142	THE STEREO CAMERA ON THE BEPICOLOMBO ESA/JAXA MISSION: A NOVEL APPROACH. , 2009, , 305-322.		16
143	EVALUATION OF AREA-BASED IMAGE MATCHING APPLIED TO DTM GENERATION WITH HIRISE IMAGES. ISPRS Annals of the Photogrammetry, Remote Sensing and Spatial Information Sciences, 0, I-4, 209-214.	0.0	16
144	The geography of Oxia Planum. Journal of Maps, 2021, 17, 621-637.	2.0	16

#	Article	IF	CITATIONS
145	Oxygen emission lines in the high resolution spectra of 9P/Tempel 1 following the Deep Impact event. Astronomy and Astrophysics, 2008, 479, 257-263.	5.1	15
146	The Agilkia boulders/pebbles size–frequency distributions: OSIRIS and ROLIS joint observations of 67P surface. Monthly Notices of the Royal Astronomical Society, 2016, 462, S242-S252.	4.4	15
147	Exposed bright features on the comet 67P/Churyumov–Gerasimenko: distribution and evolution. Astronomy and Astrophysics, 2018, 613, A36.	5.1	15
148	Surface evolution of the Anhur region on comet 67P/Churyumov-Gerasimenko from high-resolution OSIRIS images. Astronomy and Astrophysics, 2019, 630, A13.	5.1	15
149	Photometrical analysis of the Neck-Line Structure of Comet Halley. Icarus, 1989, 80, 267-279.	2.5	14
150	Observations of Mercury's exosphere: Spatial distributions and variations of its Na component during August 8, 9 and 10, 2003. Icarus, 2006, 185, 395-402.	2.5	14
151	Triple F—a comet nucleus sample return mission. Experimental Astronomy, 2009, 23, 809-847.	3.7	14
152	Hydrocode simulations of the largest crater on asteroid Lutetia. Planetary and Space Science, 2012, 66, 147-154.	1.7	14
153	Age relationships of the Rembrandt basin and Enterprise Rupes, Mercury. Geological Society Special Publication, 2015, 401, 159-172.	1.3	14
154	Possible interpretation of the precession of comet 67P/Churyumov-Gerasimenko. Astronomy and Astrophysics, 2016, 590, A46.	5.1	14
155	Loss rates of Europa× <sup>3</sup> s tenuous atmosphere. Planetary and Space Science, 2016, 130, 14-23.	1.7	14
156	Meteoroids as One of the Sources for Exosphere Formation on Airless Bodies in the Inner Solar System. Space Science Reviews, 2021, 217, 1.	8.1	14
157	First observations of the Na exosphere of Mercury with the high-resolution spectrograph of the 3.5M Telescopio Nazionale Galileo. Planetary and Space Science, 2004, 52, 1169-1175.	1.7	13
158	Long-term monitoring of comet 67P/Churyumov–Gerasimenko's jets with OSIRIS onboard Rosetta. Monthly Notices of the Royal Astronomical Society, 2017, 469, S380-S385.	4.4	13
159	Estimate of depths of source fluids related to mound fields on Mars. Planetary and Space Science, 2018, 164, 164-173.	1.7	13
160	Time evolution of dust deposits in the Hapi region of comet 67P/Churyumov-Gerasimenko. Astronomy and Astrophysics, 2020, 636, A91.	5.1	13
161	3DPD: A photogrammetric pipeline for a PUSH frame stereo cameras. Planetary and Space Science, 2021, 198, 105165.	1.7	13
162	High resolution observation of 17P/ÂHolmes during the outburst event in 2007. Astronomy and Astrophysics, 2010, 522, A82.	5.1	13

#	Article	IF	CITATIONS
163	Search for satellites near comet 67P/Churyumov-Gerasimenko using Rosetta/OSIRIS images. Astronomy and Astrophysics, 2015, 583, A19.	5.1	13
164	Neutral sodium atoms release from the surface of the Moon induced by meteoroid impacts. Monthly Notices of the Royal Astronomical Society, 2006, 367, 1067-1071.	4.4	12
165	Observations of Comet 9P/Tempel 1 around the Deep Impact event by the OSIRIS cameras onboard Rosetta. Icarus, 2007, 191, 241-257.	2.5	12
166	Modelling of the outburst on 2015 July 29 observed with OSIRIS cameras in the Southern hemisphere of comet 67P/Churyumov–Gerasimenko. Monthly Notices of the Royal Astronomical Society, 2017, 469, S178-S185.	4.4	12
167	Characterization of dust aggregates in the vicinity of the Rosetta spacecraft. Monthly Notices of the Royal Astronomical Society, 2017, 469, S312-S320.	4.4	12
168	Comparative Na and K Mercury and Moon Exospheres. Space Science Reviews, 2022, 218, 1.	8.1	12
169	Spectroscopic observations of the sodium atmosphere of the Moon. Planetary and Space Science, 1996, 44, 417-420.	1.7	11
170	Lateral ramps and strike-slip kinematics on Mercury. Geological Society Special Publication, 2015, 401, 269-290.	1.3	11
171	Asymmetries in the dust flux at Mercury. Icarus, 2016, 264, 220-226.	2.5	11
172	Opposition effect on comet 67P/Churyumov-Gerasimenko using Rosetta-OSIRIS images. Astronomy and Astrophysics, 2017, 599, A11.	5.1	11
173	Multivariate statistical analysis of OSIRIS/Rosetta spectrophotometric data of comet 67P/Churyumov-Gerasimenko. Astronomy and Astrophysics, 2017, 600, A115.	5.1	11
174	Simulations using terrestrial geological analogues to assess interpretability of potential geological features of the Hermean surface restituted by the STereo imaging Camera of the SIMBIOSYS package (BepiColombo mission). Planetary and Space Science, 2008, 56, 1079-1092.	1.7	10
175	Comet McNaught C/2006 P1: observation of the sodium emission by the solar telescope THEMIS. Astronomy and Astrophysics, 2008, 482, 293-298.	5.1	10
176	Detection of a southern peak in Mercury's sodium exosphere with the TNG in 2005. Icarus, 2009, 201, 424-431.	2.5	10
177	Photometry of dust grains of comet 67P and connection with nucleus regions. Astronomy and Astrophysics, 2016, 588, A59.	5.1	10
178	BepiColombo SIMBIO-SYS data: Preliminary evaluation for rock discrimination and recognition in both low and high resolution spectroscopic data in the visible and near infrared spectral intervals. Planetary and Space Science, 2007, 55, 1596-1613.	1.7	9
179	The Surface of Mercury as Seen by Mariner 10. Space Science Reviews, 2007, 132, 291-306.	8.1	9
180	Age dating of an extensive thrust system on Mercury: implications for the planet's thermal evolution. Geological Society Special Publication, 2015, 401, 291-311.	1.3	9

#	Article	IF	CITATIONS
181	Geometric calibration of Colour and Stereo Surface Imaging System of ESA's Trace Gas Orbiter. Advances in Space Research, 2018, 61, 487-496.	2.6	9
182	Multidisciplinary analysis of the Hapi region located on Comet 67P/Churyumov–Gerasimenko. Monthly Notices of the Royal Astronomical Society, 2019, 485, 2139-2154.	4.4	9
183	Diurnal variation of dust and gas production in comet 67P/Churyumov-Gerasimenko at the inbound equinox as seen by OSIRIS and VIRTIS-M on board Rosetta. Astronomy and Astrophysics, 2019, 630, A23.	5.1	9
184	Seasonal variations in source regions of the dust jets on comet 67P/Churyumov-Gerasimenko. Astronomy and Astrophysics, 2019, 630, A17.	5.1	9
185	The Rockyâ€Like Behavior of Cometary Landslides on 67P/Churyumovâ€Gerasimenko. Geophysical Research Letters, 2019, 46, 14336-14346.	4.0	9
186	Blocks Size Frequency Distribution in the Enceladus Tiger Stripes Area: Implications on Their Formative Processes. Universe, 2021, 7, 82.	2.5	9
187	Optical design of the High Resolution Imaging Channel of SIMBIO-SYS. Applied Optics, 2019, 58, 4059.	1.8	9
188	Characterisation of the main belt asteroid (223) Rosa. Astronomy and Astrophysics, 2021, 656, L18.	5.1	9
189	Photometric observations of comet 81P/Wild 2 during the 2010 perihelion passage. Astronomy and Astrophysics, 2012, 541, A159.	5.1	8
190	Characterization of OSIRIS NAC filters for the interpretation of multispectral data of comet 67P/Churyumov-Gerasimenko. Astronomy and Astrophysics, 2015, 583, A45.	5.1	8
191	A cone on Mercury: Analysis of a residual central peak encircled by an explosive volcanic vent. Planetary and Space Science, 2015, 108, 108-116.	1.7	8
192	Statistical analysis of the flux of micrometeoroids at Mercury from both cometary and asteroidal components. Astronomy and Astrophysics, 2016, 585, A106.	5.1	8
193	Distance determination method of dust particles using Rosetta OSIRIS NAC and WAC data. Planetary and Space Science, 2017, 143, 256-264.	1.7	8
194	Geomorphological and spectrophotometric analysis of Seth's circular niches on comet 67P/Churyumov–Gerasimenko using OSIRIS images. Monthly Notices of the Royal Astronomical Society, 2017, 469, S238-S251.	4.4	8
195	Effects of image compression and illumination on digital terrain models for the stereo camera of the BepiColombo mission. Planetary and Space Science, 2017, 136, 1-14.	1.7	8
196	The dust tail of Comet Wilson 1987VII. Astronomical Journal, 1990, 100, 1285.	4.7	8
197	Hyperspectral Data Compression Using Fully Convolutional Autoencoder. Remote Sensing, 2022, 14, 2472.	4.0	8

#	Article	IF	CITATIONS
199	Spatial variations of the sodium/potassium ratio in Mercury's exosphere uncovered by high-resolution spectroscopy. Icarus, 2010, 207, 1-8.	2.5	7
200	Innovative optical setup for testing a stereo camera for space applications. Proceedings of SPIE, 2012, , .	0.8	7
201	Radiometric model for the stereo camera STC onboard the BepiColombo ESA mission. Proceedings of SPIE, 2016, , .	0.8	7
202	Thermophysics of fractures on comet 67P/Churyumov-Gerasimenko. Astronomy and Astrophysics, 2017, 608, A121.	5.1	7
203	The big lobe of 67P/Churyumov–Gerasimenko comet: morphological and spectrophotometric evidences of layering as from OSIRIS data. Monthly Notices of the Royal Astronomical Society, 2018, 479, 1555-1568.	4.4	7
204	Pronounced morphological changes in a southern active zone on comet 67P/Churyumov-Gerasimenko. Astronomy and Astrophysics, 2019, 630, A8.	5.1	7
205	Long-term measurements of the erosion and accretion of dust deposits on comet 67P/Churyumov–Gerasimenko with the OSIRIS instrument. Monthly Notices of the Royal Astronomical Society, 2021, 504, 2895-2910.	4.4	7
206	A Mercury surface radiometric model for SIMBIO-SYS instrument suite on board of BepiColombo mission. , 2018, , .		7
207	Evaluation of an Area-Based matching algorithm with advanced shape models. International Archives of the Photogrammetry, Remote Sensing and Spatial Information Sciences - ISPRS Archives, 0, XL-4, 215-221.	0.2	7
208	Spectral Units Analysis of Quadrangle H05â€Hokusai on Mercury. Journal of Geophysical Research E: Planets, 2022, 127, .	3.6	7
209	Expected Investigation of the (65803) Didymos–Dimorphos System Using the RGB Spectrophotometry Data Set from the LICIACube Unit Key Explorer (LUKE) Wide-angle Camera. Planetary Science Journal, 2022, 3, 161.	3.6	7
210	Hale-Bopp and Its Sodium Tails. Space Science Reviews, 1999, 90, 83-89.	8.1	6
211	Characterization of the integrating sphere for the on-ground calibration of the SIMBIOSYS instrument for the BepiColombo ESA mission. Proceedings of SPIE, 2014, , .	0.8	6
212	The backscattering ratio of comet 67P/Churyumov-Gerasimenko dust coma as seen by OSIRIS onboard Rosetta. Monthly Notices of the Royal Astronomical Society, 0, , .	4.4	6
213	SIMBIO-SYS/STC stereo camera calibration: Geometrical distortion. Review of Scientific Instruments, 2019, 90, 043106.	1.3	6
214	Rosetta/OSIRIS observations of the 67P nucleus during the April 2016 flyby: high-resolution spectrophotometry. Astronomy and Astrophysics, 2019, 630, A9.	5.1	6
215	THE â€ <sup>~</sup> MOON MAPPING' PROJECT TO PROMOTE COOPERATION BETWEEN STUDENTS OF ITALY AND CHINA. International Archives of the Photogrammetry, Remote Sensing and Spatial Information Sciences - ISPRS Archives, 0, XLI-B6, 71-78.	0.2	6
216	Techniques and methods in ground-based observation of Mercury. Planetary and Space Science, 2010, 58, 61-78.	1.7	5

#	Article	IF	CITATIONS
217	Stereo Camera for satellite application: A new testing method. , 2014, , .		5
218	Is the Linné impact crater morphology influenced by the rheological layering on the Moon's surface? Insights from numerical modeling. Meteoritics and Planetary Science, 2017, 52, 1388-1411.	1.6	5
219	Performance evaluation of the SIMBIO-SYS Stereo Imaging Channel on board BepiColombo/ESA spacecraft. Measurement: Journal of the International Measurement Confederation, 2019, 135, 828-835.	5.0	5
220	Observational constraints to the dynamics of dust particles in the coma of comet 67P/Churyumov–Gerasimenko. Monthly Notices of the Royal Astronomical Society, 2021, 504, 4687-4705.	4.4	5
221	GAUSS - genesis of asteroids and evolution of the solar system. Experimental Astronomy, 0, , 1.	3.7	5
222	A novel optical design for planetary surface stereo-imaging: preliminary design of the stereoscopic imaging channel of SIMBIOSYS for the BepiColombo ESA mission. , 2006, 6265, 714.		4
223	A New Stereo Algorithm based on Snakes. Photogrammetric Engineering and Remote Sensing, 2011, 77, 495-507.	0.6	4
224	Ghost images determination for the stereoscopic imaging channel of SIMBIOSYS for the BepiColombo ESA mission. Proceedings of SPIE, 2011, , .	0.8	4
225	Quantitative analysis of isolated boulder fields on comet 67P/Churyumov-Gerasimenko. Astronomy and Astrophysics, 2019, 630, A15.	5.1	4
226	Optical performance evaluation of the high spatial resolution imaging camera of BepiColombo space mission. Optics and Laser Technology, 2021, 141, 107172.	4.6	4
227	Modelling reconstruction and boulder size-frequency distribution of a young (<5ÂMyr) landslide located in Simud Vallis floor, Mars. Icarus, 2022, 375, 114850.	2.5	4
228	The Io Sodium Cloud: Comparison between Observations and Numerical Models. Icarus, 1998, 131, 138-151.	2.5	3
229	MEMORIS: a wide angle camera for the BepiColombo mission. Advances in Space Research, 2004, 33, 2182-2188.	2.6	3
230	Performance evaluation of DTM area-based matching reconstruction of Moon and Mars. Proceedings of SPIE, 2012, , .	0.8	3
231	A stable auroral red arc over Europe. Astronomy and Geophysics, 2012, 53, 1.16-1.18.	0.2	3
232	The JANUS camera onboard JUICE mission for Jupiter system optical imaging. Proceedings of SPIE, 2014, ,	0.8	3
233	DTM generation from STC-SIMBIO-SYS images. , 2015, , .		3
234	Distortion definition and correction in off-axis systems. Proceedings of SPIE, 2015, , .	0.8	3

#	Article	IF	CITATIONS
235	Geometrical distortion calibration of the stereo camera for the BepiColombo mission to Mercury. Proceedings of SPIE, 2016, , .	0.8	3
236	Temporal evolution of the permanent shadowed regions at Mercury poles: applications for spectral detection of ices by SIMBIOSYS-VIHI on BepiColombo mission. Monthly Notices of the Royal Astronomical Society, 2020, 498, 1308-1318.	4.4	3
237	Excitation and ionization of sodium in meteoroid impacts on the Moon. Astronomy and Astrophysics, 2002, 394, 723-727.	5.1	3
238	Subpixel-Scale Topography Retrieval of Mars Using Single-Image DTM Estimation and Super-Resolution Restoration. Remote Sensing, 2022, 14, 257.	4.0	3
239	la nube di sodio su io. Rendiconti Lincei, 1990, 1, 235-244.	2.2	2
240	The dust environment of comet Levy 1990XX. Planetary and Space Science, 1994, 42, 263-268.	1.7	2
241	Spectrophotometric variegation of the layering in comet 67P/Churyumov-Gerasimenko as seen by OSIRIS. Astronomy and Astrophysics, 2019, 630, A16.	5.1	2
242	The pre-launch distortion definition of SIMBIO-SYS/STC stereo camera by rational function models. , 2018, , .		2
243	A high-spectral-resolution catalog of emission lines in the visible spectrum of comet C/2020 F3 (NEOWISE). Astronomy and Astrophysics, 2021, 656, A160.	5.1	2
244	Optical design performance of the stereo channel for Simbiosys onâ€board the Bepicolombo ESA mission. , 2019, , .		2
245	An analysis of possible asteroids flyby for the ESA JUICE mission. Planetary and Space Science, 2022, 216, 105476.	1.7	2
246	The SSDC Role in the LICIACube Mission: Data Management and the MATISSE Tool. Planetary Science Journal, 2022, 3, 126.	3.6	2
247	Observing Mercury: from Galileo to the stereo camera on the BepiColombo mission. Proceedings of the International Astronomical Union, 2010, 6, 213-218.	0.0	1
248	A method for studying the effects of thermal deformations on optical systems for space application. Proceedings of SPIE, 2010, , .	0.8	1
249	Correction to "Mercury's geochronology revised by applying Model Production Function to Mariner 10 data: Geological implications― Geophysical Research Letters, 2010, 37, n/a-n/a.	4.0	1
250	A preliminary optical design for the JANUS camera of ESA's space mission JUICE. , 2014, , .		1
251	The CaSSIS imaging system: optical performance overview. , 2016, , .		1
252	Performances of the SIMBIO-SYS Stereo Imaging Channel (STC) on Board BepiColombo/ESA Spacecraft. , 2018, , .		1

#	Article	IF	CITATIONS
253	Radiometric calibration of the SIMBIO-SYS STereo imaging Channel. CEAS Space Journal, 2019, 11, 485-496.	2.3	1
254	Phase-curve analysis of comet 67P/Churyumov-Gerasimenko at small phase angles. Astronomy and Astrophysics, 2019, 630, A11.	5.1	1
255	Martian Ice Revealed by Modeling of Simple Terraced Crater Formation. Journal of Geophysical Research E: Planets, 2020, 125, e2019JE006108.	3.6	1
256	Development of a simulator of the SIMBIOSYS suite onboard the BepiColombo mission. Monthly Notices of the Royal Astronomical Society, 2020, 491, 1673-1689.	4.4	1
257	Laboratory characterization of HYPSOS, a novel 4D remote sensing instrument. , 2021, , .		1
258	Spectral response of the stereo imaging channel of SIMBIO-SYS on-board the ESA BepiColombo Mission. , 2019, , .		1
259	SIMBIOSYS-STC ready for launch: a technical recap. , 2019, , .		1
260	SIMBIO-SYS STC ready for the first light: the radiometric calibration. , 2019, , .		1
261	Mercury's Surface Composition and Character as Measured by Ground-Based Observations. Space Sciences Series of ISSI, 2008, , 217-249.	0.0	1
262	ESTIMATE OF DTM DEGRADATION DUE TO IMAGE COMPRESSION FOR THE STEREO CAMERA OF THE BEPICOLOMBO MISSION. International Archives of the Photogrammetry, Remote Sensing and Spatial Information Sciences - ISPRS Archives, 0, XLI-B4, 471-478.	0.2	1
263	SIMBIO-SYS Near Earth Commissioning Phase: a step forward toward Mercury. , 2019, , .		1
264	Lunam 2000 (Lunar Atmosphere Mission). Earth, Moon and Planets, 1999, 85/86, 487-495.	0.6	0
265	Benefits of the Proposed Magia Mission for Lunar Geology. Earth, Moon and Planets, 2010, 107, 267-297.	0.6	Ο
266	Effects of thermal deformations on the sensitivity of optical systems for space application. , 2010, , .		0
267	The narrow angle camera of the MPCS suite for the MarcoPolo ESA Mission: requirements and optical design solutions. Proceedings of SPIE, 2010, , .	0.8	Ο
268	MarcoPolo-R narrow angle camera: a three-mirror anastigmat design proposal with a smart finite conjugates refocusing optical system. Proceedings of SPIE, 2012, , .	0.8	0
269	Preliminary LSF and MTF determination for the stereo camera of the BepiColombo mission. Proceedings of SPIE, 2014, , .	0.8	0
270	Thin-film optical pass band filters based on new photo-lithographic process for CaSSIS FPA detector on Exomars TGO mission: development, integration, and test. Proceedings of SPIE, 2016, , .	0.8	0

#	Article	IF	CITATIONS
271	Meteor Showers on the Lunar Atmosphere. , 2001, , 479-486.		0
272	Lunam 2000 (Lunar Atmosphere Mission). , 2001, , 487-495.		0
273	OSIRIS: The Scientific Camera System Onboard Rosetta. , 2009, , 1-67.		0
274	Hale-Bopp and Its Sodium Tails. , 1999, , 83-89.		0
275	Optical design and performance of the Stereoscopic Imaging Channel for the ESA BepiColombo mission. , 2017, , .		0